

CHALMERS



Transient Simulation of GaN HEMTs

Thesis for Erasmus Mundus Master's degree in Nanoscience and Nanotechnology

SHREETU SHRESTHA

Microwave Electronics Laboratory
Department of Microtechnology and Nanoscience
CHALMERS UNIVERSITY OF TECHNOLOGY
Gothenburg, Sweden, 2013



KU LEUVEN

Thesis for Erasmus Mundus Master's degree in Nanoscience and
Nanotechnology

Transient Simulation of GaN HEMTs

SHREETU SHRESTHA

Microwave Electronics Laboratory

Department of Microtechnology and Nanoscience - MC2

CHALMERS UNIVERSITY OF TECHNOLOGY

Göteborg, Sweden 2013

Transient Simulation of GaN HEMTs

Shreetu Shrestha

© Shreetu Shrestha, 2013

Microwave Electronics Laboratory

Department of Microtechnology and Nanoscience - MC2

Chalmers University of Technology

SE-412 96 Göteborg

Sweden

Telephone + 46 (0)31-772 1000

This report is written in \LaTeX

Chalmers Reproservice

Göteborg, Sweden 2013

Abstract

Subthreshold drain leakage can be suppressed in GaN HEMTs by intentionally doping the GaN buffer with deep acceptor dopants such as C and Fe or by using a double heterostructure. In this thesis, both concepts, doping and using double heterostructure were investigated using numerical device simulation. The main focus was on the study of transient electrical behaviour and the understanding of trapping behaviour of deep acceptor dopants which causes current collapse. It was found that current collapse is dependent on dopant concentration and is worse with Fe doping than with C doping. These results were explained by considering the potential barrier formed in the GaN buffer due to electron trapping. Transistors with an undoped GaN channel layer on top of a doped GaN buffer layer had a small current collapse but much a higher drain current.

Keywords: GaN/AlGaN, HEMT, current collapse

Contents

Abstract	i
1 Introduction	1
2 Theory	3
2.1 Polarisation	3
2.2 AlGa _N /Ga _N HEMT	4
2.3 Trap Dynamics	5
2.4 Current Collapse	6
3 Simulation	9
3.1 Simulation software	9
3.2 Device Structure and parameters	10
3.3 Physical models	11
3.4 Trap Definition	13
4 Results	15
4.1 AlGa _N /Ga _N : [C] HEMTs	15
4.1.1 DC characterisation	16
4.1.2 Transient pulsed simulation	17
4.2 AlGa _N /Ga _N : [Fe] HEMTs	22
4.2.1 DC characterisation	22
4.2.2 Transient pulsed simulation	24
4.2.3 Trap energy level and thermal effects	25
4.3 AlGa _N /Ga _N /Ga _N : [C] HEMTs	27
4.3.1 DC characterisation	28
4.3.2 Transient pulsed simulation	28
4.4 AlGa _N /Ga _N /AlGa _N DH-HEMTs	30
4.4.1 DC characterisation	30
4.4.2 Transient pulsed simulation	32
5 Conclusion	35
Acknowledgements	36
References	39

Chapter 1

Introduction

GaN based HEMTs have attracted considerable attention over the last decade. First fabricated in 1993 [1], GaN based HEMTs have been commercially available since 2005 [2]. The major application areas today include RF and microwave electronics [3].

GaN has several advantages over conventional III-V semiconductors. With a wide bandgap of 3.4 eV, GaN based HEMTs can be operated at high electric fields and high temperatures. The electron density in the channel is also higher in comparison to other III-V semiconductors like GaAs. Although the low-field mobility of electrons in GaN bulk is lower than that of GaAs, GaN has a larger saturation velocity. Due to these qualities, GaN HEMTs are suitable candidates for high power and high voltage applications.

One of the concerns with GaN HEMTs is the subthreshold drain leakage at high drain-source bias. Electrons can punch through the GaN buffer at high electric fields. This effect can be suppressed by intentionally doping the GaN buffer with deep acceptor impurities such as C and Fe which trap electrons and reduce current leakage. These traps however, also cause unwanted memory effects resulting in current collapse; a phenomenon described as a temporary decrease in current due to trapping of electrons. It is important to address such nonlinear behaviour because it severely limits the output power performance [4]. As an alternative to doping, a double heterostructure which confines electrons in the channel can also be used to minimize current leakage.

In this thesis, both concepts, doping and using double heterostructure are investigated using numerical device simulation. The main focus is on the study of transient electrical behaviour and understanding of trapping dynamics which causes current collapse. A brief background of GaN HEMTs and trap dynamic is given in Chapter 2. The simulation setup, models and parameters are covered in Chapter 3. The result section, Chapter 4, is divided into four groups; AlGaN/GaN:[C] HEMTs, AlGaN/GaN:[Fe] HEMTs, AlGaN/GaN/GaN:[C] HEMTs and AlGaN/GaN/AlGaN HEMTs. DC and transient pulsed simulation results are discussed for all the four device structures. Finally, the results are summarized and a conclusion is drawn in Chapter 5.

Chapter 2

Theory

2.1 Polarisation

The unit cell of GaN with hexagonal wurtzite structure is shown in Fig. 2.1. The spacing between two hexagonal lattice planes is defined by c , the distance of atoms in the hexagonal plane is defined by a and the bond length along the c -axis is defined by u [5]. For an ideal hexagonal wurtzite structure, the lattice constant ratio c/a is $\sqrt{8/3}$, and u is $3/8$ [6]. However, due to the internal

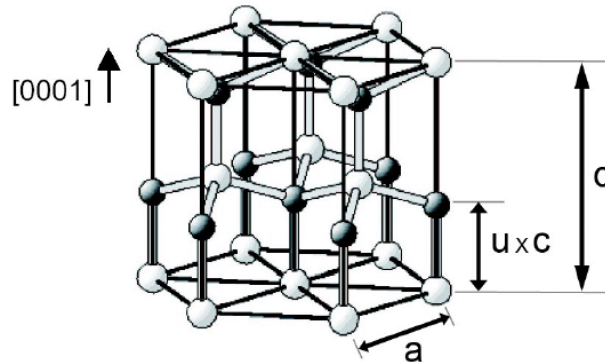


Figure 2.1: Hexagonal wurtzite crystal structure of GaN. Picture taken from [7]

asymmetry along the c -axis of GaN crystal the c/a ratio differs from the ideal value giving rise to spontaneous polarization [8]. This is an intrinsic property of the material and exists even in bulk.

Piezoelectric polarization, on the other hand, is induced by mechanical strain. The lattice constant of AlGaN is smaller than that of GaN. Due to this difference the thin AlGaN layer is strained which gives rise to piezoelectric polarization.

2.2 AlGaN/GaN HEMT

The high polarization in AlGaN/GaN heterostructure results in a high electric field which produces a high charge density at the interface. Free electrons tend to compensate this polarization induced charge. A two-dimensional electron gas (2DEG) is thus formed at the AlGaN/GaN interface provided that the conduction band offset is reasonably high [9].

Unlike other conventional HEMTs, intentional doping is not required in GaN HEMTs due to high internal polarisation. A sheet carrier concentration of 10^{13} cm^{-3} can be achieved without any intentional doping. There are different theories explaining the origin of the electrons in 2DEG but it is generally agreed that they come from the donor states on the AlGaN surface [10, 11].

Fig. 2.2 shows the device structure of a typical AlGaN/GaN HEMT. The current flows from the Ohmic drain contact through the 2DEG channel to the Ohmic source contact. The size of the channel is controlled by the voltage applied at the Schottky gate contact. The sheet carrier concentration n_s varies along the channel as [12]

$$n_s(x) = \frac{\sigma(x)}{e} - \left(\frac{\epsilon_0 \epsilon(x)}{de^2} \right) [e\phi_b(x) + E_F(x) - \Delta E_c(x)], \quad (2.1)$$

where $\sigma(x)$ is the positive piezoelectric sheet charge density, ϵ is the dielectric constant of AlGaN, d is the width of the AlGaN barrier, $e\phi_b$ is the Schottky barrier of the gate contact, $E_F(x)$ is the Fermi level with respect to the GaN conduction band and $\Delta E_c(x)$ is the conduction band offset at the interface. AlGaN/GaN HEMTs are normally on device. Therefore, a negative gate voltage larger than the threshold voltage has to be applied to pinch off the channel as shown in Fig. 2.3.

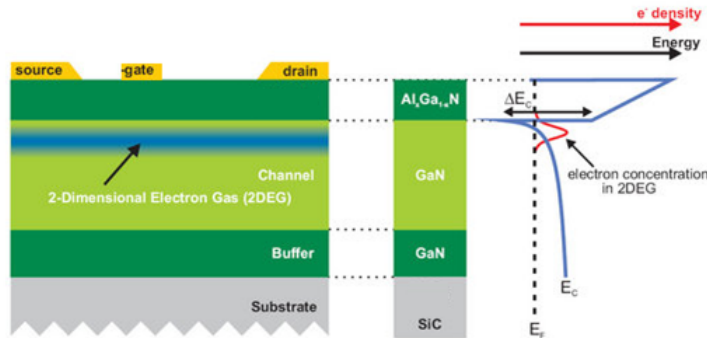


Figure 2.2: AlGaN/GaN HEMTs device structure with energy of conduction band (blue) and electron density (red). Picture taken from [13].

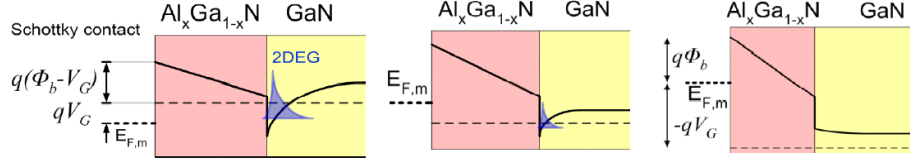


Figure 2.3: 2DEG modulation when $V_{gs} > 0$ (left), $V_{gs} < 0$ (middle) and $V_{gs} < V_{th}$. Picture taken from [14].

2.3 Trap Dynamics

Traps can be created on the surface or in the bulk of the heterostructure by external dopants, impurities and intrinsic defects. In this thesis only the traps created by external doping will be considered. External dopants can introduce localized states with energy level E_T in the forbidden energy gap of the semi-conducting material. Charge carriers can be captured or emitted from these levels. Assuming that a system is in equilibrium, the probability of capture and emission would depend on the Fermi level. The probability that a trap is occupied by an electron f_t is given by [15]

$$f_t = \frac{1}{1 + \exp\left(\frac{E_t - E_f}{kT}\right)}, \quad (2.2)$$

where E_t is the energy level of the trap. The electron capture rate at the same location as the trap is

$$c^n = v_{th}\sigma_n n, \quad (2.3)$$

where v_{th} is the thermal velocity, σ_n is the capture cross section for electrons and n is the number of electrons. The electron capture rate R^1 is proportional to the number of unoccupied traps [15]

$$R^1 = c^n N_t (1 - f_t), \quad (2.4)$$

where N_t is the number of traps. Similarly, the electron emission rate R^2 is proportional to the number of occupied traps [15]

$$R^2 = e^n N_t f_t, \quad (2.5)$$

where e^n is the electron emission rate given that a trap is occupied.

When the system is in thermal equilibrium, the forward and reverse process balance each other. Therefore, R^1 and R^2 are equal in equilibrium [15].

$$v_{th}\sigma_n n N_t (1 - f_t) = e^n N_t f_t \quad (2.6)$$

Since $n = n_i \exp\left(\frac{E_f - E_i}{kT}\right)$,

$$v_{th}\sigma_n n_i \exp\left(\frac{E_f - E_i}{kT}\right) N_t (1 - f_t) = e^n N_t f_t \quad (2.7)$$

From Eq. 2.2, $\frac{1-f_t}{f_t} = \exp \frac{E_t - E_f}{kT}$, so

$$e^n = v_{th} \sigma_n n_i \exp \frac{E_t - E_i}{kT} \quad (2.8)$$

Since Eq. [2.8] does not depend on the electron occupation probability f_t (and the Fermi level), it is valid even in nonequilibrium conditions although it was derived using equilibrium assumptions. This equation shows that there is an exponential relationship between trap energy level and emission rate. Traps with energy level closer to the conduction band have a higher electron emission rate.

2.4 Current Collapse

Current collapse refers to the temporary reduction in drain current after the application of a high drain-source bias [4]. Fig. 2.4 shows an average of about 800 pulsed measurement results of AlGaIn/GaN HEMT for drain voltage pulsed from 15 V to 30 V. When the drain voltage is pulsed to 30 V for 0 μ s, electrons from the channel are accelerated and penetrate the GaN buffer where they get captured by traps. Due to the trapping of electrons, the drain current decreases.

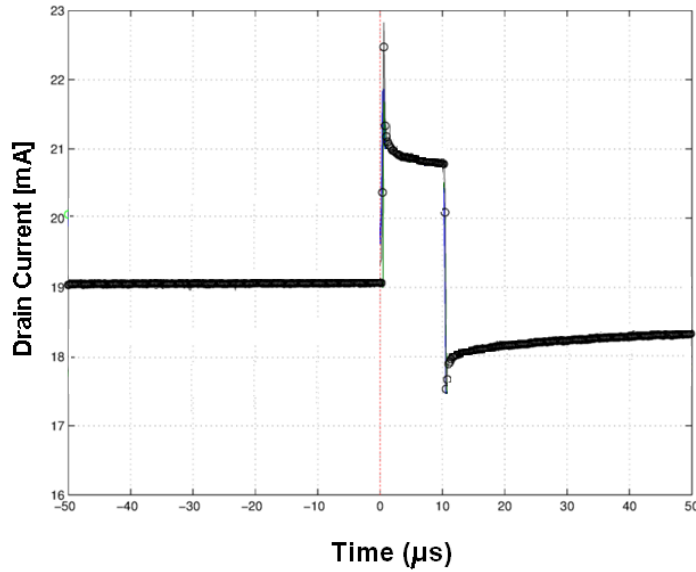


Figure 2.4: Average measured transient drain current response at $V_{gs} = -1.8$ V, V_{ds} pulsed from 15 V to 30 V. Measurements taken by Daniel Niessen.

The electrons remain trapped for a while even after the drain voltage is pulsed back to 15 V. Therefore, the drain current level after the pulse is lower than that before the pulse. The trapped electrons can be emitted by stimulus like

light or heat which assists them to overcome the emission barrier and return to the channel [4]. Thus, this is a recoverable phenomenon as the drain current eventually comes back to its equilibrium level.

Current collapse is observed in other semiconductor devices like AlGaAs/GaAs HEMTs as well. However, it is more problematic in GaN based HEMTs due to the high operating voltage and the relative immaturity of GaN technology.

Chapter 3

Simulation

3.1 Simulation software

Synopsys TCAD was used to perform numerical device simulations. Synopsys provides a number of tools for simulating devices, managing simulation tasks and analysing simulation results [16]. The following tools were used in this project:

Sentaurus structure editor (SSE) creates 2D and 3D device structures. The structure of a device is approximated by a "mesh" consisting of a large number of elements. Continuous physical quantities like electric field and temperature are converted into discrete elements of a mesh. A higher mesh density gives a more accurate and precise result but at the cost of a higher computation time. Therefore, denser meshes were used only in the regions where the current density and electric field was expected to be high as shown in Fig.3.1. Meshing strategies and doping profiles were defined using SSE.

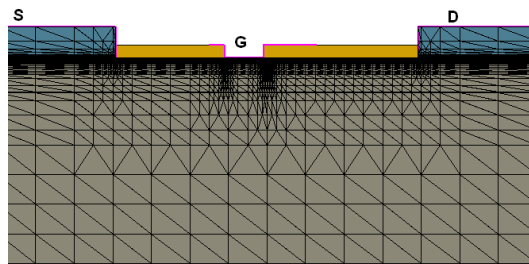


Figure 3.1: HEMT structure with Mesh created in SSE. The mesh density is higher at the interface.

Sentaurus Device (SD) solves the Poisson's equation and the carrier continuity equations for given boundary conditions and device structure. The software uses numerical solvers which iterates repeatedly until a solution with desired accuracy is obtained [17]. Models defining mobility, bandgap, recombination and other physical properties were specified in SD.

Visualisation software Inspec was used to plot I-V characteristics. Sentaurus Visual (SV) was used to visualise 2D output data from the simulation for current density, trap occupation, band diagram and others.

Sentaurus work bench (SWB) provides a graphical user interface to integrate all other Synopsys tools. SWB was used as a framework to create, manage, execute and analyse TCAD simulations [16].

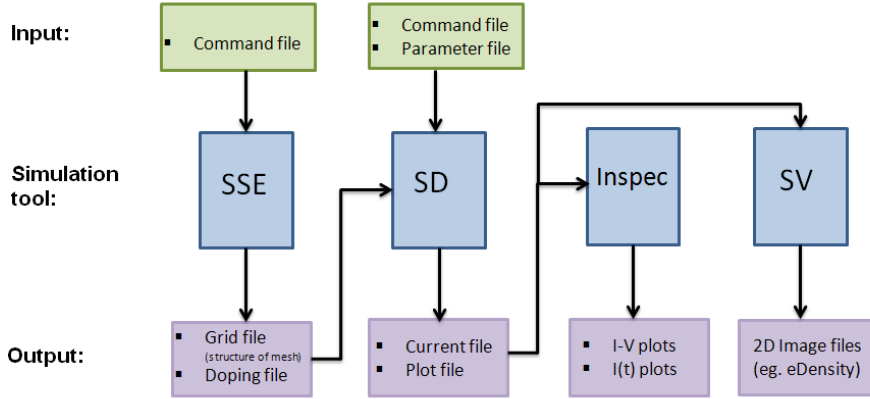


Figure 3.2: Simulation tool workflow with important input and output files

3.2 Device Structure and parameters

The schematic of the simulated AlGa_{0.25}GaN/GaN HEMT structure is shown in Fig. 3.3. 20 nm thick Al_{0.25}Ga_{0.75}N barrier layer on top of 2 μm thick GaN buffer layer was simulated. Some properties of the materials used are given in Table. 3.1.

Table 3.1: Material properties of GaN, Al_{0.25}Ga_{0.75}N and SiC [18–22]

		GaN	Al _{0.25} Ga _{0.75} N	SiC
Relative Permittivity	to <i>c</i> -axis	10.4	10.13	9.8
	⊥ to <i>c</i> -axis	9.5	9.06	9.8
Bandgap at 300 K (eV)		3.40	4.10	3.19
Electron affinity at 300 K (eV)		3.44	3.05	4.10

The polarization effect was modelled with a fixed positive density charge of $1.39 \times 10^{13} \text{ cm}^{-2}$ at the AlGa_{0.25}GaN/GaN interface and a fixed negative charge density of $3.20 \times 10^{13} \text{ cm}^{-2}$ at the AlGa_{0.25}GaN/Si₃N₄ interface [9].

A donor trap sheet density of $1 \times 10^{14} \text{ cm}^{-2}$ was set at the Si₃N₄/AlGa_{0.25}GaN-barrier interface. The surface barrier (ϕ_s), which is the difference between the AlGa_{0.25}GaN-barrier conduction band and Fermi level at the surface, was modelled as a single donor energy level equivalent to 1.78 eV below conduction band [23]. Drain

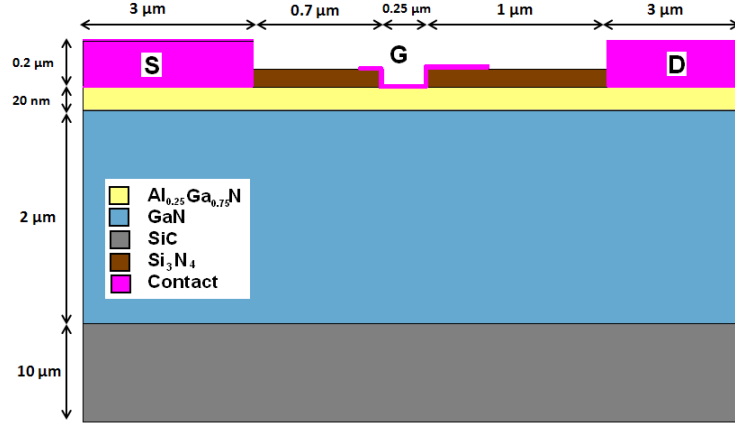


Figure 3.3: Simulated device structure (not drawn to scale)

and source contacts were modelled as Ohmic metal/semiconductor interface on heavily doped AlGa_{0.25}N region. A doping concentration of $1 \times 10^{20} \text{ cm}^{-3}$ was set in the AlGa_{0.25}N regions under the contacts.

The interface between two materials were modelled as heterointerface. Fermi-Dirac distribution statistics and Shockley-Read-Hall recombination were enabled. The temperature was fixed to 298 K and background doping was not considered.

3.3 Physical models

Sentaurus device allows us to choose from a variety of different physical models. Some important models that were used in this thesis are described below

Drift Diffusion model

The drift diffusion (DD) model is based on the method of moments solution of the Boltzmann's transport equation (BTE) [24]. The basic idea of BTE is that the time rate of change of probability distribution function, f , is proportional to the scattering events [24].

$$\frac{df}{dt} = \left\{ \frac{\partial f}{\partial t} \right\}_{scattering} \quad (3.1)$$

By applying relaxation time approximation, BTE can be expressed as [24]

$$\frac{df}{dt} = \nabla_r f \cdot \mathbf{v}_g + \nabla_k f \cdot \frac{\mathbf{F}}{\hbar} = \frac{f - f_0}{\tau} \quad (3.2)$$

where \mathbf{v}_g is the group velocity of distribution, ∇_r and ∇_k are the gradient in real space and momentum, \mathbf{F} is the applied force and f_0 is the distribution function

at thermal equilibrium. Moments of the BTE are obtained by multiplying Eq.3.2 by a quantity to be conserved and integrating over all k space [24]. The first moment, where the quantity to be conserved is the particle number, gives the current continuity equations

$$\nabla \cdot \mathbf{J}_n = qR + q \frac{\partial n}{\partial t} \quad (3.3)$$

$$-\nabla \cdot \mathbf{J}_p = qR + q \frac{\partial p}{\partial t} \quad (3.4)$$

where \mathbf{J}_n is the electron current density, \mathbf{J}_p is the hole current density and R is the net recombination rate. The DD equation takes into account the first two moments of BTE. The current density is expressed as a sum of drift and diffusion term as [25]

$$\mathbf{J}_n = nq\mu_n \nabla \mathbf{E} + qD_n \nabla n \quad (3.5)$$

$$\mathbf{J}_p = pq\mu_p \nabla \mathbf{E} - qD_p \nabla p \quad (3.6)$$

where μ_n and μ_p are the electron and hole mobility, and D_n and D_p are the corresponding diffusion coefficients. μ_n and D_n are related by the Einstein relation [25]

$$D_n = \mu_n \frac{kT}{q} \quad (3.7)$$

From 3.7, 3.5 and 3.6, the current density can be finally expressed in terms of quasi-Fermi potentials as [25]

$$\mathbf{J}_n = -nq\mu_n \nabla \phi_n \quad (3.8)$$

$$\mathbf{J}_p = -pq\mu_p \nabla \phi_p \quad (3.9)$$

SD also offers other transport models. The Hydrodynamic model (HD), for example, considers the first 4 moments of BTE and is thus physically more accurate. However, to reduce the complexity and save computation time, only the basic drift-diffusion model was used in this project.

Mobility model

Fig. 3.4 shows the velocity of various semiconductors as a function of electric field. The electron velocity in Si and SiC increases with an increase in electric field and then saturates at high fields. The electron velocity in AlGaIn/GaN interface however, does not saturate but continues to increase at slower rate and then decreases.

Therefore, a mobility model with two linear regions described in [27] was used for AlGaIn/GaN. This model takes into account the electric field and also the lattice temperature. The mobility is given by

$$\mu(T, E) = \frac{\mu_{LF}}{\sqrt[\beta]{1 + \left(\frac{\mu_{LF} E}{v_0 + \mu_{HF} E}\right)^\beta}} \quad (3.10)$$

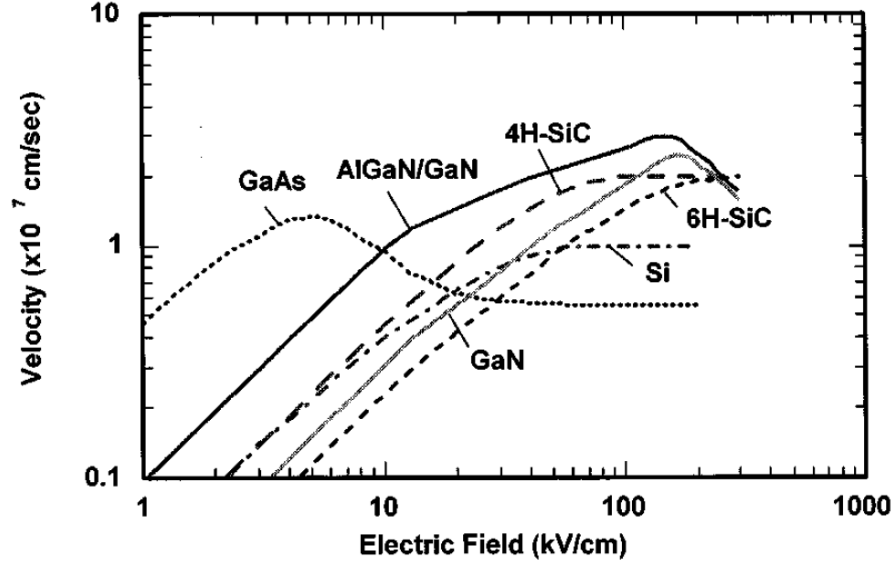


Figure 3.4: Electron velocity as a function of electric field for various semiconductors ($N_d = 10^{17} \text{ cm}^{-3}$). Picture taken from [26]

$$= \frac{\mu_{LF0} \left(\frac{T}{T_0}\right)^{-\mu_{LFexp}}}{\beta_0 \left(\frac{T}{T_0}\right)^{-\beta_{exp}} \sqrt{1 + \left(\frac{\mu_{LF0} \left(\frac{T}{T_0}\right)^{-\mu_{LFexp}} E}{v_{00} \left(\frac{T}{T_0}\right)^{-v_{0exp}} + \mu_{HF0} \left(\frac{T}{T_0}\right)^{-\mu_{HFexp}} E}\right)^{\beta_0 \left(\frac{T}{T_0}\right)^{-\beta_{exp}}}} \quad (3.11)$$

where E is the electric field parallel to the current, μ_{LF} is the differential mobility at low electric fields, v_0 is the intersection of extrapolated high field with the y -axis, and β governs the smoothness of the transition between the low-field and high-field regions. The temperature dependence is modelled by the exponents μ_{LFexp} , μ_{HFexp} , v_{0exp} and β_{exp} . β_0 , μ_{LF0} , μ_{HF0} and v_{00} are values at T_0 [27].

3.4 Trap Definition

Acceptor type traps were simulated in the GaN buffer layer. These traps are neutral when unoccupied and carry the charge of one electron when occupied. The traps were uniformly distributed in the GaN buffer. The energy of the traps was set to a single specified level. In literature, different values of the trap energy level for C [28] and Fe [29] doping can be found. While the exact value of the trap energy level is in debate, there is a general agreement that C traps form acceptor levels in the lower half of the energy gap and Fe traps form acceptor levels in the upper half of the energy gap. In this thesis, C and Fe trap energy levels were set to 0.9 eV [30] and 2.9 eV [31] above the valance

band respectively. The capture cross section was set to $1 \times 10^{-15} \text{ cm}^2$ for both C and Fe traps [32].

The electron capture rate from the conduction band c_C^n at a location same as the trap is simulated as [33]

$$c_C^n = \sigma_n v_{th} n, \quad (3.12)$$

where σ_n is the electron capture cross section, v_{th} is the thermal velocity and n is the electron density. Similarly, the electron emission rate to the conduction band is simulated as [33]

$$e_C^n = \sigma_n v_{th} N_C \exp\left[\frac{(E_{trap} - E_C)}{kT}\right], \quad (3.13)$$

where N_C is the electron density of state, E_{trap} is the trap energy level and E_C is the conduction band energy.

Chapter 4

Results

Four different transistor were investigated; AlGa_N/Ga_N:_[C] HEMTs, AlGa_N/Ga_N:_[Fe] HEMTs, AlGa_N/Ga_N/Ga_N:_[C] HEMTs and AlGa_N/Ga_N/AlGa_N. DC and transient pulsed simulation results for all four transistors will be discussed in this section.

4.1 AlGa_N/Ga_N:_[C] HEMTs

The simulated I-V curves for AlGa_N/Ga_N HEMTs with 20 nm thick Al_{0.25}Ga_{0.75}N barrier layer and 2 μm thick Ga_N buffer layer are shown in Fig. 4.1.

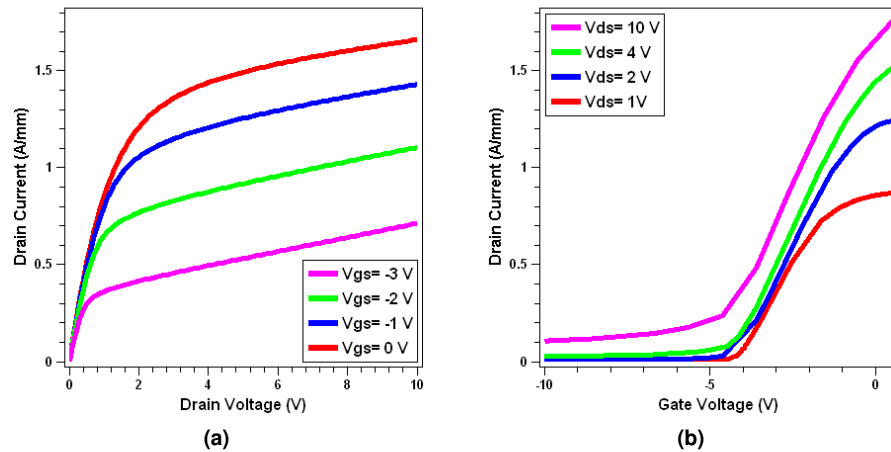


Figure 4.1: Simulated I-V curves for AlGa_N/Ga_N HEMTs (a) $I_{DS}-V_{DS}$ (b) $I_{DS}-V_{GS}$

Subthreshold drain leakage current can be observed for $V_{ds} = 10$ V in Fig. 4.1b due to the punch-through effect. Even when the channel is pinched off, electrons

can flow through the GaN buffer under the depleted channel at high V_{ds} . This leakage current can be suppressed by doping the GaN buffer with deep acceptor impurities which trap electrons. Two commonly used dopants in GaN HEMTs are C and Fe. In this section, the DC and transient characteristics with C doped GaN buffer will be discussed.

4.1.1 DC characterisation

Fig. 4.2 shows the I-V curves for AlGaIn/GaN HEMTs with $1 \times 10^{16} \text{ cm}^{-3}$ C dopants in the GaN buffer. It can be seen that drain current is lower with C doping than without any doping. The drain leakage current at $V_{ds} = 10 \text{ V}$ is suppressed and the output resistance is higher.

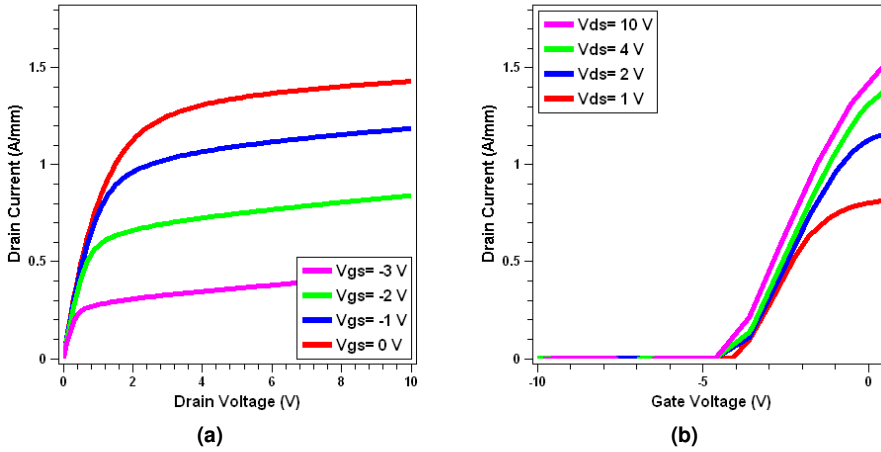


Figure 4.2: I-V curves for AlGaIn/GaN HEMTs with 1×10^{16} C doped GaN buffer (a) I_{ds} - V_{ds} (b) I_{ds} - V_{gs}

Similar plots were simulated for AlGaIn/GaN HEMTs with $1 \times 10^{17} \text{ cm}^{-3}$ C doped GaN buffer. The I-V curves for the three different cases are compared in Fig.4.3. It can be seen that the drain current further decreases with $1 \times 10^{17} \text{ cm}^{-3}$ C doping. The V_{th} increases from -4.1 V for 1×10^{16} C doping to -3.4 V for 1×10^{17} doping.

These results can be explained by considering the trapping behaviour of C impurities. The traps created by C dopants in the GaN buffer capture electrons from the 2DEG channel. Therefore, the electron density is lower which results in a lower drain current. With more dopants, more electrons from the channel are trapped in the buffer. Therefore, the drain current decreases as the C concentration increases.

The increase in V_{th} and output resistance with higher doping is due to the increase in buffer potential as shown in Fig. 4.4a. As mentioned earlier, occupied traps carry a charge of one electron. This negative charge in the buffer increases the potential barrier. As a result, the subthreshold drain leakage through the

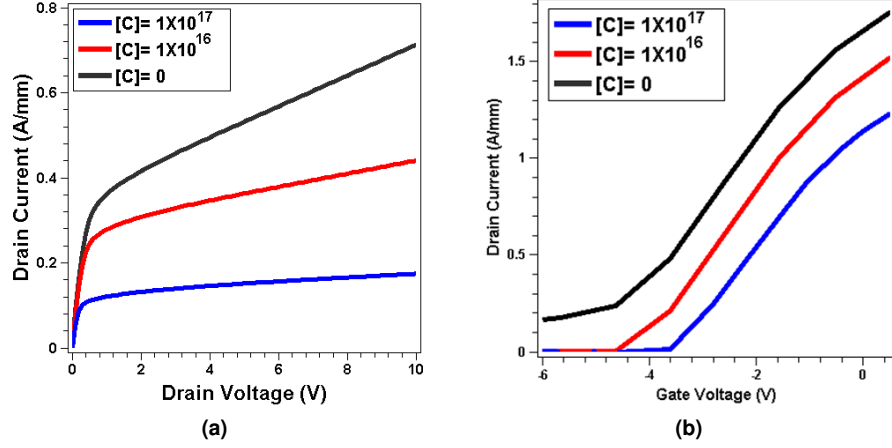


Figure 4.3: I-V curves for AlGaN/GaN HEMTs with no doping, $1 \times 10^{16} \text{ cm}^{-3}$ and $1 \times 10^{17} \text{ cm}^{-3}$ C doped GaN buffer (a) I_{ds} - V_{ds} at $V_{gs} = -3 \text{ V}$ (b) I_{ds} - V_{gs} at $V_{ds} = 10 \text{ V}$

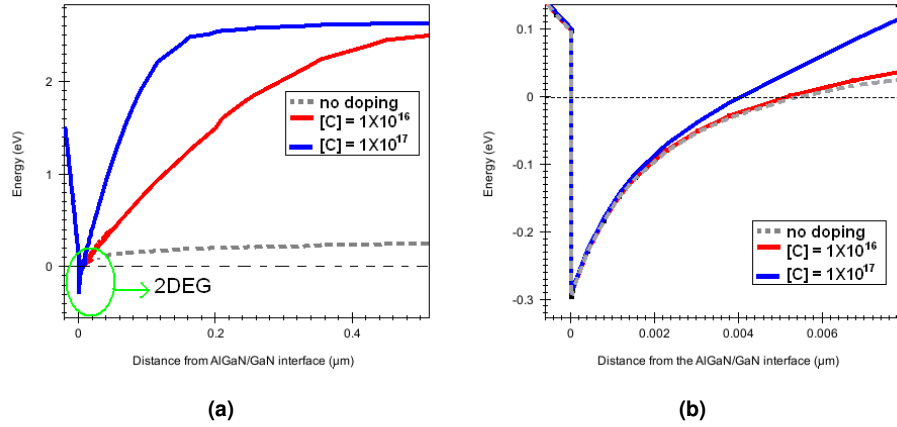


Figure 4.4: (a) Energy diagram of conduction band at steady state for AlGaN/GaN HEMTs with no doping, $1 \times 10^{16} \text{ cm}^{-3}$ and $1 \times 10^{17} \text{ cm}^{-3}$ C doped GaN buffer as a function of distance from the AlGaN/GaN interface (b) 2DEG

buffer is suppressed and V_{th} is increased. Although a higher dopant concentration is desirable to achieve a higher V_{th} , it also results in a lower drain current. Therefore, there is a trade off between higher V_{th} and higher drain current.

4.1.2 Transient pulsed simulation

For transient simulations, the drain voltage was pulsed from 15 V to 30 V for a period of 10 μs as shown in Fig.4.5a. The ramping time was set to 10 ns. The

gate voltage was kept constant at -4 V.

Fig.4.5b shows the transient simulation results for AlGaIn/GaN HEMTs with 1×10^{16} C doping and no doping. It can be seen that without any doping, the drain current follows the drain voltage linearly. The current after the pulse is exactly equal to the current before the pulse. This however, is not the case with 1×10^{16} C traps. When the drain voltage is ramped to 30 V, the current reaches a maximum value and then decreases. A small peak can be observed as the current decreases rapidly during the first $2 \mu\text{s}$. The drain current after the pulse also goes down by 12.1% .

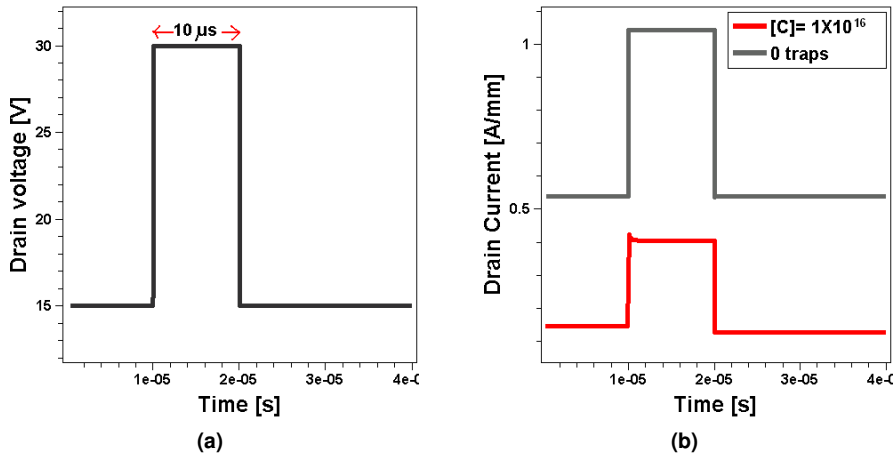


Figure 4.5: (a) Drain voltage pulsed from $V_{dsq} = 15$ V to $V_{dsp} = 30$ V (b) $I_{ds}(t)$ for AlGaIn/GaN HEMTs with 1^{16} C doping and no doping at $V_{gs} = -4$ V

This can be explained by considering trap dynamics. Before the pulse, there is an equilibrium between the process of electron capture and emission. When the drain voltage is ramped to 30 V, electrons gain more energy and spill over in the buffer as shown in Fig. 4.6(b). It takes some time for the electrons to get trapped. In the beginning, traps closer to the interface are filled quickly resulting in a rapid decrease in current. Gradually over time, traps located deeper in the bulk are filled.

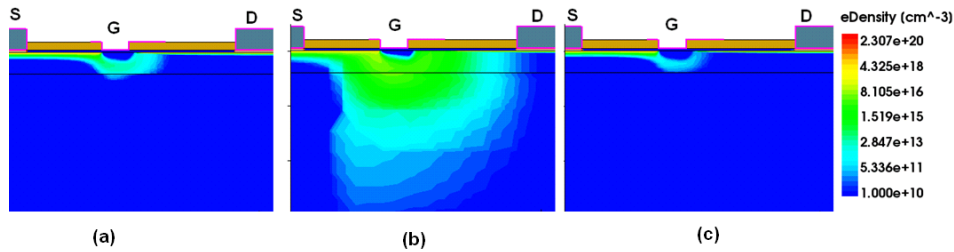


Figure 4.6: Electron density (a) before, (b) during and (c) after the drain voltage pulse at $V_{gs} = -4$ V.

Once captured, the electrons remain in the traps unless they gain enough energy to go back. When the drain voltage is ramped down to 15 V, a lot of electrons which were trapped during the pulse still remain trapped in the buffer. Fig. 4.7 shows the difference in the density of trapped electrons before and after the pulse. The blue region represents the area where traps that were unoccupied before the pulse were occupied after the pulse. It can be seen that more electrons get trapped below the gate region after the pulse.

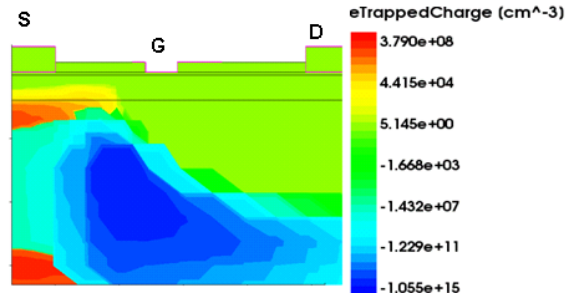


Figure 4.7: The difference in occupied trap density before and after the pulse

Therefore the electron density in the channel after the pulse is lower than before as shown in Fig. 4.6. This phenomenon is known as current collapse. If the simulations are run for a longer time it can be observed that the current gradually increases back to the equilibrium position as the captured electrons are emitted from the traps.

Duration of pulse

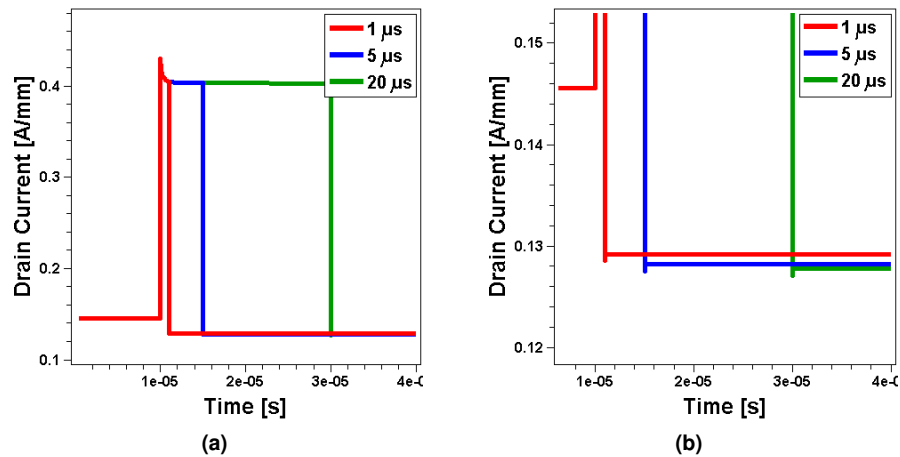


Figure 4.8: (a) $I_{ds}(t)$ when V_{gs} was pulsed from 15 V to 30 V for 1 μ s, 5 μ s and 20 μ s at a constant $V_{ds} = -4$ V (b) zoom in of (a) showing current collapse

Fig. 4.8 shows the transient drain current response when the drain voltage

was pulsed from 15 V to 30 V for 1 μ s, 5 μ s and 20 μ s. The V_{gs} was kept constant at -4 V. For drain voltage pulse duration of 1 μ s, 5 μ s and 20 μ s, the current collapse was 11.3%, 12.0% and 12.3% respectively. The current collapse increases with pulse duration because more electrons are trapped over a longer period of time. However, the rate of electrons being trapped decreases gradually as more and more traps are filled. Therefore the difference in current collapse between 1 μ s and 5 μ s is 0.7% while the difference is only 0.3% between 5 μ s and 20 μ s although the time duration difference is longer.

V_{DS} Dependence

Fig. 4.9a shows the drain current when V_{ds} was pulsed from 5 V to 15 V, 30 V and 60 V. The V_{gs} was kept constant at -4 V. It can be seen that for a higher pulse drain voltage, the peak in the drain current is sharper. The reason for this is that at higher drain voltage electrons have more energy and can penetrate deeper in the buffer in a shorter duration of time. As a result, more electrons get trapped in the buffer. Therefore, the current collapse is higher for a higher V_{dsp} as shown in Fig. 4.9b. For V_{dsp} 15 V, 30 V and 60 V, the current collapse is 6.9%, 63.8% and 90.2% respectively.

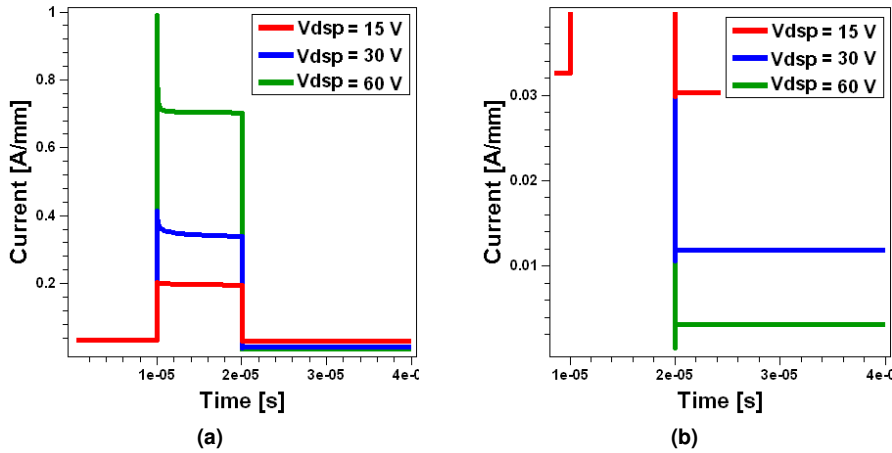


Figure 4.9: (a) $I_{ds}(t)$ for $V_{dsp} = 15$ V, 30 V and 60 V at $V_{gs} = -4$ V (b) Current collapse

V_{GS} Dependence

Fig. 4.10a shows the drain current when the drain voltage was pulsed from 15 V to 30 V for $V_{gs} = -2$ V, -3 V and -4 V. The percentage current collapse for different V_{gs} is shown in Fig. 4.10b. It can be observed that as the gate voltage decreased, the current collapse increases. This is because, with a more negative gate voltage the channel is closer to pinch off and there are fewer electrons in the channel. The electron density for different V_{gs} can be seen in Fig. 4.11. For a

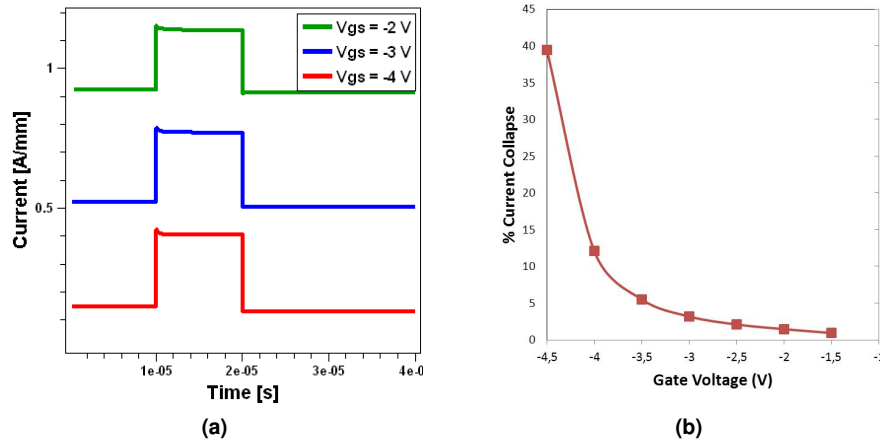


Figure 4.10: (a) $I_{ds}(t)$ for $V_{gs} = -2$ V, -3 V and -4 V (b) Percentage current collapse for different V_{gs} . V_{ds} pulsed from 15 V to 30 V.

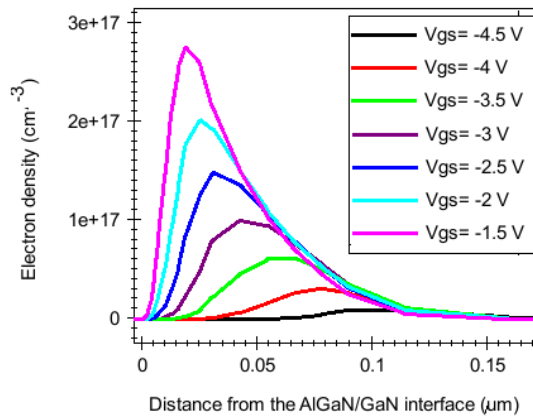


Figure 4.11: Electron density near the AlGaN/GaN interface for different V_{gs}

lower gate voltage there are fewer electrons in the channel and they are sparsely distributed. Therefore, a higher fraction of electrons get trapped.

Doping concentration

Fig. 4.12a shows the drain current for AlGaN/GaN HEMTs with $1 \times 10^{16} \text{ cm}^{-3}$ and $1 \times 10^{17} \text{ cm}^{-3}$ C doping concentration in the GaN buffer. Again the V_{ds} was pulsed from 15 V to 30 V and current collapse for different V_{gs} was calculated. The percentage current collapse for different C doping concentration can be seen in Fig. 4.12b. It can be seen that the current collapse increases when the doping concentration is increased from $0.8 \times 10^{16} \text{ cm}^{-3}$ to $1 \times 10^{16} \text{ cm}^{-3}$.

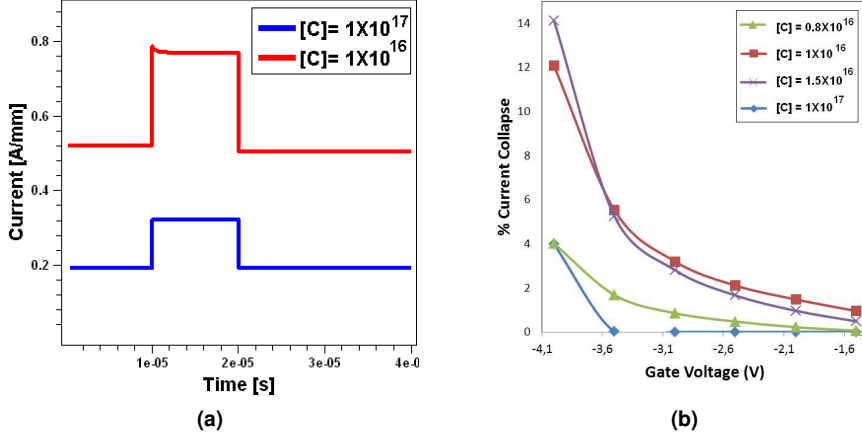


Figure 4.12: (a) $I_{ds}(t)$ with $1 \times 10^{16} \text{ cm}^{-3}$ and $1 \times 10^{17} \text{ cm}^{-3}$ C doping concentration $V_{gs} = -3 \text{ V}$ (b) Percentage current collapse for different V_{gs} . V_{ds} pulsed from 15 V to 30 V.

However, when the dopant concentration was increased further to $1.5 \times 10^{16} \text{ cm}^{-3}$ and $1 \times 10^{17} \text{ cm}^{-3}$ the current collapse decreases. This result was rather unexpected since it was presumed that the current collapse would be worse with more traps.

These results can be explained by considering the screening effect of occupied traps. Traps filled with electrons are negatively charged. As more and more traps become occupied it gets increasingly difficult for electrons from the channel to penetrate the GaN buffer. The negative charge of the occupied traps confine electrons in the channel resulting in fewer electrons being trapped.

Fig. 4.13a shows the density of occupied traps after the pulse for $1 \times 10^{16} \text{ cm}^{-3}$ and $1 \times 10^{17} \text{ cm}^{-3}$ C doping. It can be seen that for $1 \times 10^{16} \text{ cm}^{-3}$ C doping, traps located deep in the bulk are fully occupied. For $1 \times 10^{17} \text{ cm}^{-3}$ C doping however, fewer traps deep in the buffer are occupied. This can be explained by the conduction band energy diagram shown in Fig. 4.13b. For $1 \times 10^{16} \text{ cm}^{-3}$ C traps, the conduction band energy near the interface is lower. For $1 \times 10^{17} \text{ cm}^{-3}$ C traps, the higher density of occupied traps near the channel increases the conduction band energy and confines electrons more effectively. Thus it can be said that after a certain number of traps are occupied, the screening effect of occupied traps dominates and limits the electron spillover into the GaN buffer.

4.2 AlGaN/GaN:[Fe] HEMTs

4.2.1 DC characterisation

Fig. 4.14 shows the I-V curves for AlGaN/GaN HEMTs with different concentrations of C and Fe doping in the GaN buffer. Similar to the case with C

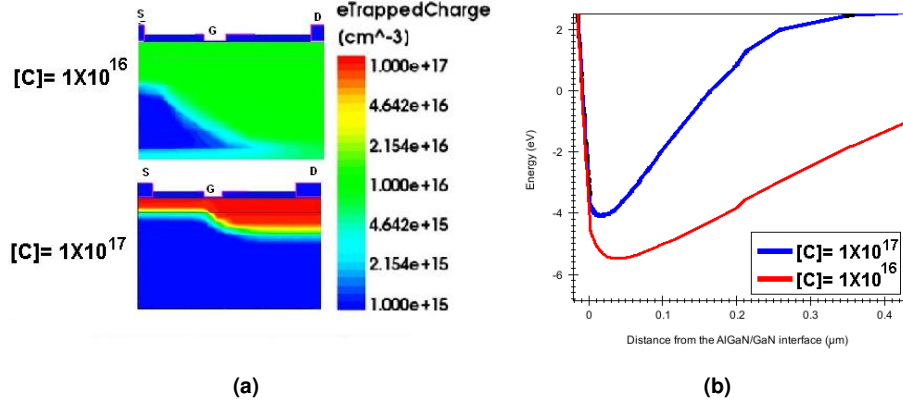


Figure 4.13: (a) Density of trapped electrons after pulse for 10^{16} cm^{-3} C doping (top) and 10^{17} cm^{-3} C doping (bottom) (b) Energy of conduction band at $V_{gs} = -3 \text{ V}$ near the drain edge of gate before pulse

doping, the drain current is lower with a higher Fe doping concentration. The V_{th} also increases from -4.3 V for $1 \times 10^{16} \text{ cm}^{-3}$ Fe doping to -3.8 V for $1 \times 10^{17} \text{ cm}^{-3}$ Fe doping.

In comparison to C doping, the drain current is slightly higher and the V_{th} is lower with Fe doping. This is because the Fe trap energy level (2.9 eV from the valance band) is higher than C trap energy level (0.9 eV from the valance band). Since Fe trap energy level is closer to the conduction band the probability that a Fe trap is occupied is lower than that for C trap. As a result, with Fe doping fewer electrons are trapped and the electron density in the channel is higher which results in a higher drain current. also increases from -4.3 V for 1×10^{16}

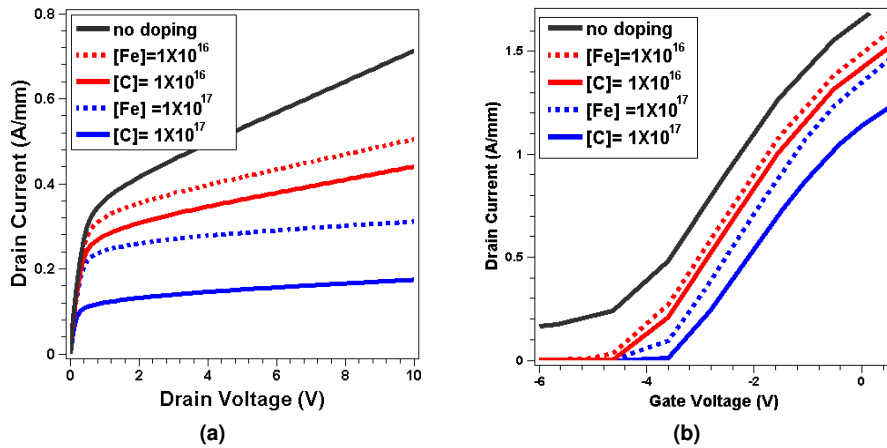


Figure 4.14: I-V curves for AlGaN/GaN HEMTs without doping, $1 \times 10^{16} \text{ cm}^{-3}$ and $1 \times 10^{17} \text{ cm}^{-3}$ doping concentration of C and Fe (a) I_{ds} - V_{ds} at $V_{gs} = -3 \text{ V}$ (b) I_{ds} - V_{gs} at $V_{ds} = 10 \text{ V}$

cm^{-3} Fe doping to -3.8 V for $1 \times 10^{17} \text{ cm}^{-3}$ Fe doping.

The conduction band energy diagram for C and Fe doping is shown in Fig. 4.15a. Due to the shallower energy level of Fe traps, the increase in conduction band energy is lower with Fe doping. The lower bulk potential along with higher electron density gives a lower V_{th} for devices with Fe doping.

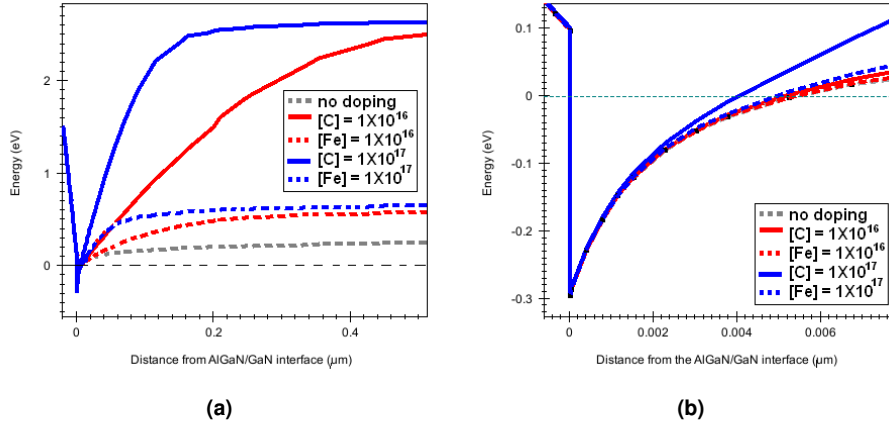


Figure 4.15: (a) Energy diagram of conduction band at steady state for AlGaIn/GaN HEMTs with no doping, $1 \times 10^{16} \text{ cm}^{-3}$ and $1 \times 10^{17} \text{ cm}^{-3}$ C and Fe doped GaN buffer as a function of distance from the AlGaIn/GaN interface (b) zoom in of potential well

4.2.2 Transient pulsed simulation

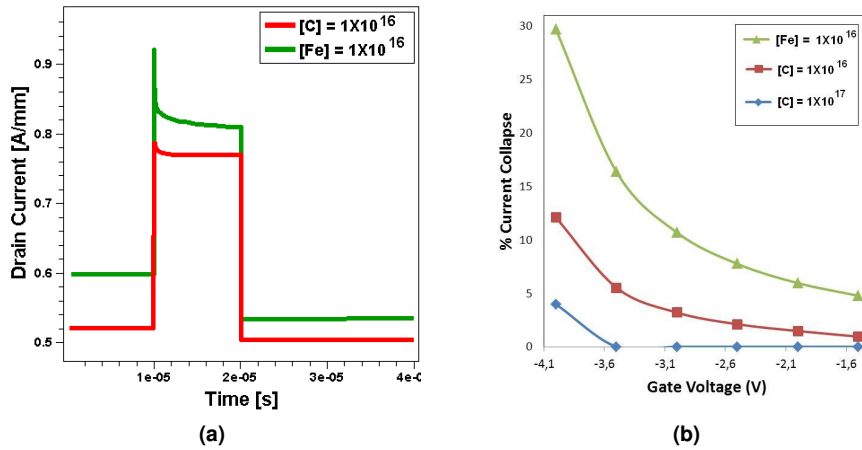


Figure 4.16: (a) $I_{ds}(t)$ for C and Fe doping at $V_{gs} = -3$ V. (b) Percentage current collapse for different V_{gs} . V_{ds} pulsed from 15 V to 30 V.

Fe traps have energy level closer to the conduction band than C traps. Therefore,

Fe traps emit electrons faster and the probability that Fe traps are unoccupied is higher. Since fewer Fe traps are occupied at any given time, the drain current is higher with Fe doping in comparison to C doping as shown in Fig. 4.16a.

The percentage current collapse with $1 \times 10^{16} \text{ cm}^{-3}$ Fe and C doping for different V_{gs} is shown in Fig.4.16b. Since the potential barrier in the bulk with Fe traps is lower, more electrons can spill over in the buffer during the pulse and get trapped. As a result, the peak rise in current is bigger and the current collapse is higher with Fe doping.

Fig. 4.17 shows the density of trapped electrons for Fe (top) and C (bottom) traps. It can be clearly seen that for Fe traps the density of trapped electrons is higher after the pulse while the difference is not so obvious for C traps.

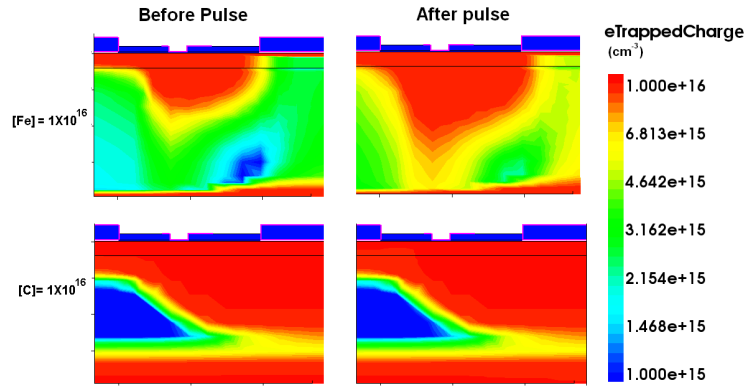


Figure 4.17: Density of trapped electrons before and after the pulse for 10^{16} cm^{-3} Fe (top) and C traps(bottom) at $V_{gs} = -3 \text{ V}$.

Fe doping concentration

Fig. 4.18a shows the percentage current collapse for Fe and C doping. It can be seen that unlike C doping, for Fe doping the current collapse increases when the doping concentration is increased to $1 \times 10^{17} \text{ cm}^{-3}$. This can be explained by considering the conduction band diagram shown in Fig. 4.18b. Due to the shallow nature of Fe traps, although the conduction band energy increases for $1 \times 10^{17} \text{ cm}^{-3}$ doping it is still not high enough to confine electrons in the channel. The electrons can thus penetrate the GaN buffer and get trapped as shown in Fig. 4.19. Therefore the current collapse increases for $1 \times 10^{17} \text{ cm}^{-3}$ Fe doping because although more electrons get trapped near the channel, electron confinement is not effective and electrons still spill over in the bulk.

4.2.3 Trap energy level and thermal effects

In earlier sections, the differences in the transient drain current response with C and Fe doping in the GaN buffer have been discussed. Since the only difference in our simulations between C and Fe doping is the energy level of

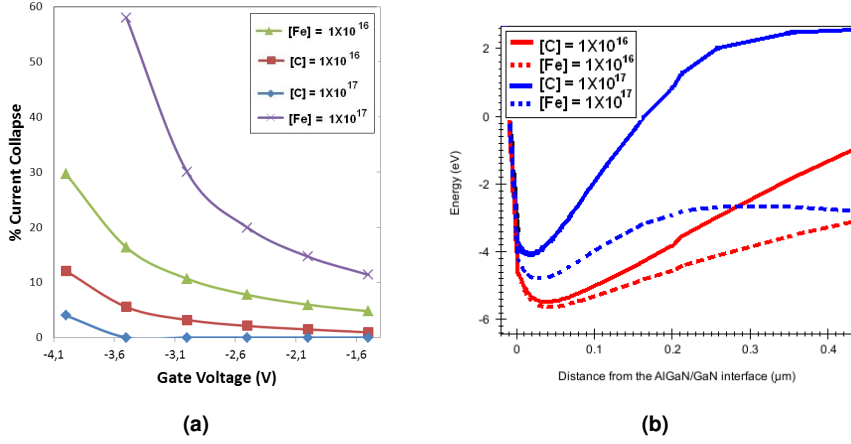


Figure 4.18: (a) Percentage current collapse for 10^{16} cm⁻³ and 10^{17} cm⁻³ C and Fe doping (b) Energy of conduction band at $V_{gs} = -3$ V near the drain edge of gate before pulse

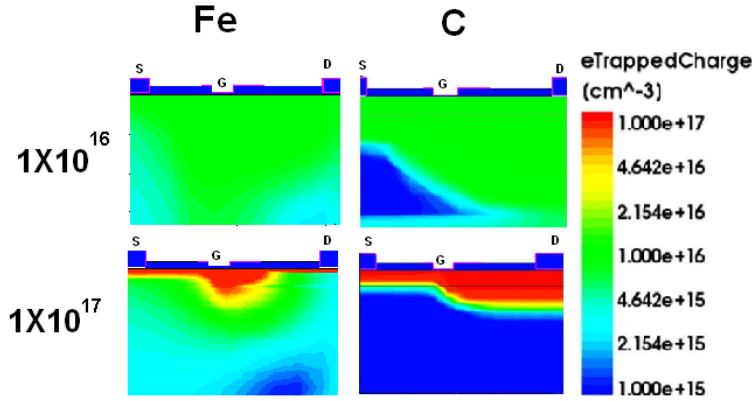


Figure 4.19: Density of trapped electrons before and after the pulse for 10^{16} cm⁻³ and 10^{17} cm⁻³ C and Fe doping at $V_{gs} = -3$ V

traps formed, it can be said that the transient response is very sensitive to the trap energy level. Fig. 4.20 shows the drain current for 10^{16} cm⁻³ traps with different energy levels. It can be seen that for traps with energy level closer to the conduction band, the drain current recovers to the equilibrium level faster. The reason for this is that there is an exponential relationship between emission of trapped electrons and the difference between the trap and the conduction band energy level (as given in Eq. 3.13). Therefore, electrons are emitted faster from shallower traps and as a result the drain current goes back to the equilibrium level in a shorter duration of time.

The emission of trapped electrons is also thermally activated (as given in Eq. 3.13). Fig. 4.21 shows drain current and average lattice temperature for 1×10^{16} cm⁻³ trap concentration with trap energy level $E_T = 3$ eV. Without thermal

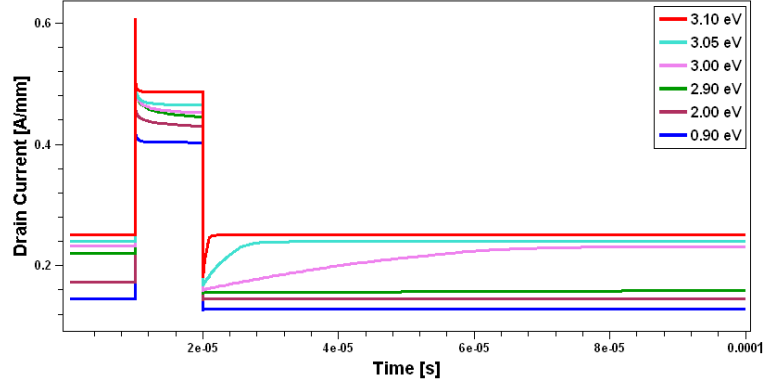


Figure 4.20: $I_{ds}(t)$ for $1 \times 10^{16} \text{ cm}^{-3}$ trap concentration with trap energy level, $E_T = 0.9 \text{ eV}, 2 \text{ eV}, 2.9 \text{ eV}, 3 \text{ eV}, 3.05 \text{ eV}$ and 3.1 eV at $V_{gs} = -4 \text{ V}$.

effects the lattice temperature is set to a fixed value of 298 K. It can be seen that with thermal effects the maximum lattice temperature increases from 340 K before the pulse to 430 K during the pulse. Therefore, before the pulse fewer electrons are trapped and the equilibrium current level is higher. During the pulse the drain current decreases faster because of mobility degradation of electrons at higher temperature. Similarly after the pulse, the drain current recovers faster because of the additional thermal energy which assists the emission of trapped electrons. The electron mobility also increases as the device cools down.

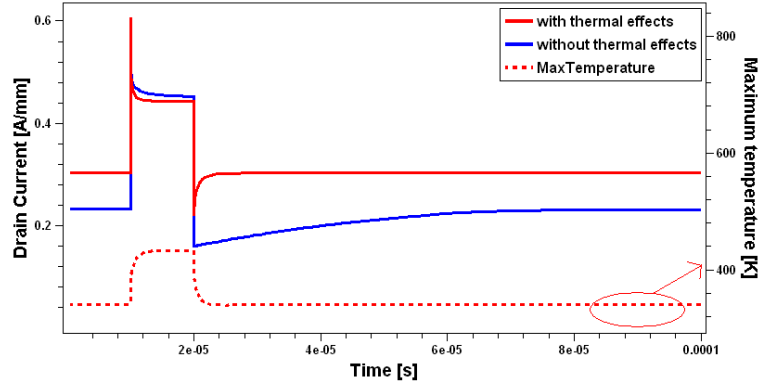


Figure 4.21: $I_{ds}(t)$ for $1 \times 10^{16} \text{ cm}^{-3}$ trap concentration with trap energy level, $E_T = 3 \text{ eV}$ with and without thermal effects at $V_{gs} = -4 \text{ V}$.

4.3 AlGaIn/GaN/GaN:[C] HEMTs

In Section 4.1, it was found that current collapse is negligible with $1 \times 10^{17} \text{ cm}^{-3}$ C doping in the GaN buffer. However, the drain current with $1 \times 10^{17} \text{ cm}^{-3}$

C doping is low. In order to minimize current collapse and increase the drain current at the same time, a thin undoped GaN channel layer on top of C doped GaN buffer was used as shown in Fig. 4.22a. Since the doped layer is further away from the channel, fewer electrons are trapped. In this section the DC and transient pulsed simulation results for AlGa_{0.25}Ga_{0.75}N/GaN/GaN:[C] with thickness of the undoped GaN layer $d = 50$ nm, 200 nm and 500 nm were simulated. The total thickness of the buffer was kept constant. 1×10^{17} cm⁻³ C doping was used in the GaN:[C] layer.

4.3.1 DC characterisation

Fig. 4.23 shows the I-V curves for different thickness of undoped GaN layer. It can be seen that as we increase the thickness of the undoped layer, the drain current increases. The V_{th} is -3.4 V, -3.8 V, -3.9 V and -4.2 V for $d = 0$ nm, 50 nm, 200 nm and 500 nm respectively. This is because with a thicker undoped GaN layer, there are fewer traps and they are located further away from the channel. As a result the electron density in the channel is higher but at the same time the V_{th} is lower since the potential barrier underneath the channel is lower as shown in Fig. 4.22b.

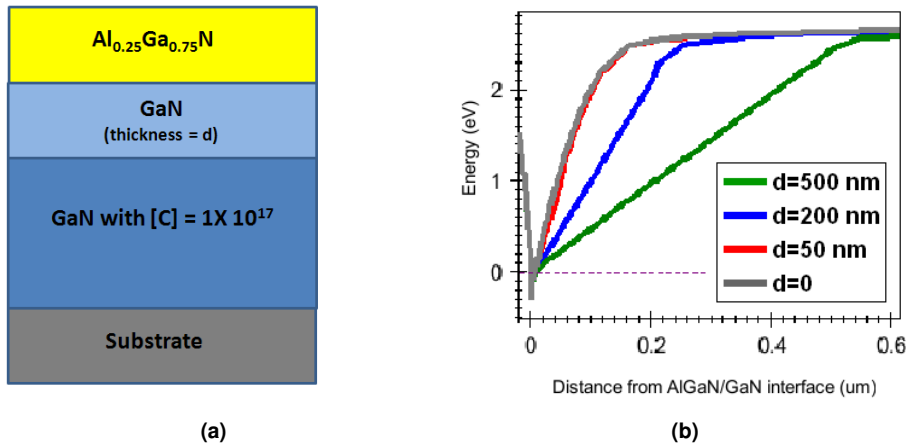


Figure 4.22: (a) AlGa_{0.25}Ga_{0.75}N/GaN/GaN:[C] HEMTs device structure (b) Energy diagram of conduction band for $d = 0, 50$ nm, 200 nm and 500 nm.

4.3.2 Transient pulsed simulation

Fig. 4.24a shows the drain current for $d = 0, 50$ nm, 200 nm and 500 nm. The percentage current collapse with a higher value of d is higher as shown in Fig. 4.24b. This is because with a thicker undoped layer the traps are located further away from the channel and so fewer electrons are trapped before the pulse. As a result, the buffer potential and the screening effect of trapped electrons is lower. When the pulse is turned on, a larger number of electrons can penetrate the buffer and get trapped.

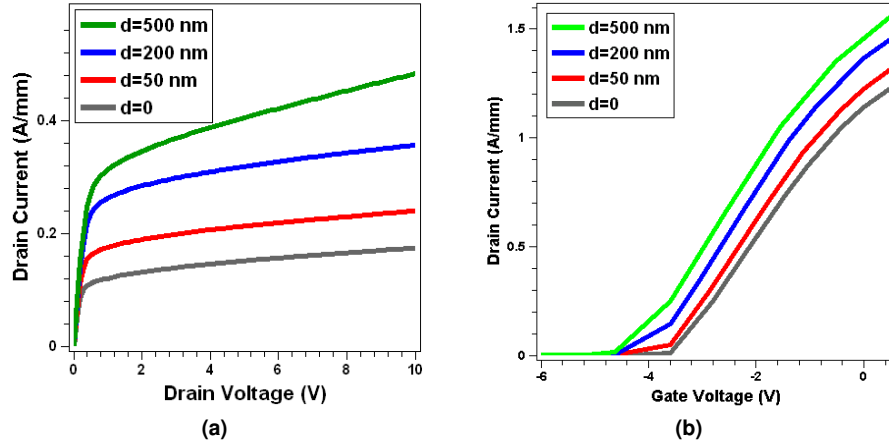


Figure 4.23: I-V curves for AlGaN/GaN/GaN:[C] HEMTs with different thickness of undoped GaN layer d (a) I_{ds} - V_{ds} curves at $V_{gs} = -3$ V (b) I_{ds} - V_{gs} curves at $V_{ds} = 10$ V

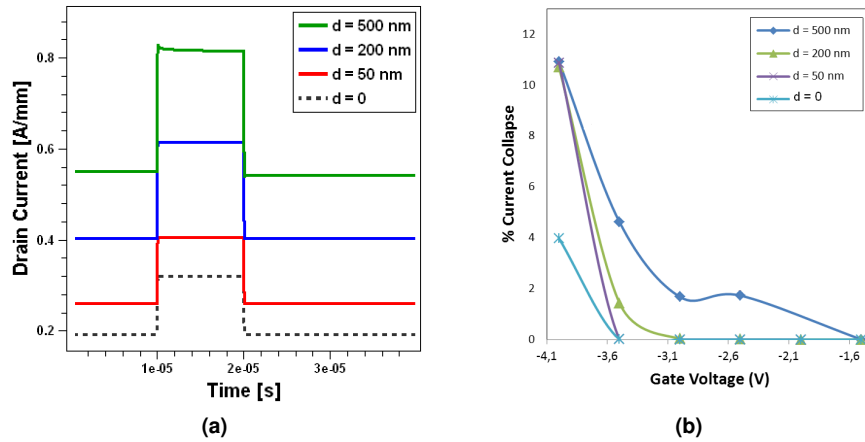


Figure 4.24: (a) Current collapse for different thickness of undoped layer d at $V_{gs} = -3$ V (b) Percentage current collapse as a function of V_{gs}

Fig. 4.25a shows that the density of trapped electrons before and after the pulse is the same for $d = 0$ at $V_{gs} = -3.5$ V. But for $d = 500$ nm the density of trapped electrons increases after the pulse.

At higher V_{gs} however the percentage current collapse goes to 0 again. This is because since the V_{gs} is higher, there are more electrons captured before the pulse to provide a better electron confinement. Therefore, fewer electrons are trapped during the pulse. Fig. 4.25b shows that there is no change in density of trapped electrons for $d = 500$ nm at $V_{gs} = -1.5$ V.

Although AlGaN/GaN/GaN:[C] HEMTs with thicker undoped GaN layer suffer

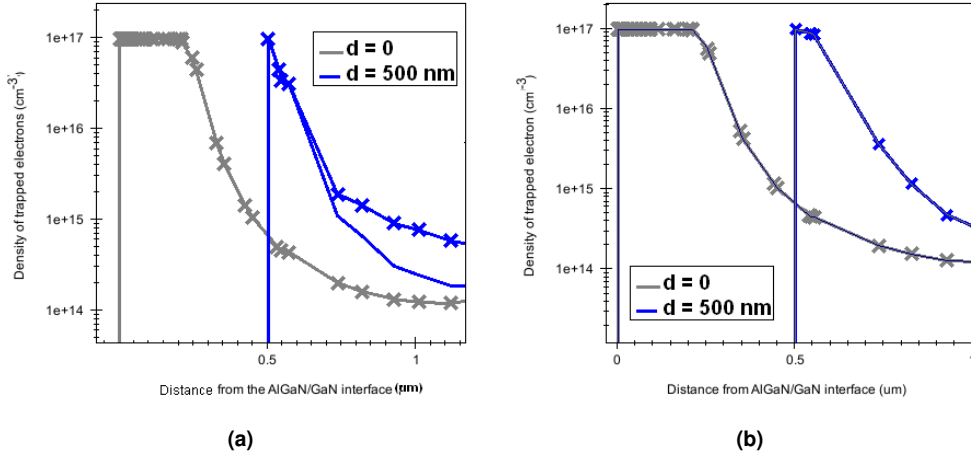


Figure 4.25: Density of trapped electrons as a function of distance before the pulse (smooth line) and after the pulse (with x marker) at (a) $V_{gs} = -3.5$ V (b) $V_{gs} = -1.5$ V

from higher current collapse (at lower V_{gs}) and have a lower V_{th} in comparison to uniformly doped buffer, they also give a higher conductivity. The drain current with $d = 500$ nm at $V_{gs} = -3$ V is about 200% higher than with $d = 0$. Considering this, it might still be worthwhile to use an undoped layer.

Furthermore, the mobility degradation with higher doping has not been considered in the mobility model used in this project. In reality, mobility of electrons in the channel decreases due to scattering caused by collision with dopants. If this is taken into account the current without an undoped GaN layer will be even lower.

4.4 AlGaIn/GaN/AlGaIn DH-HEMTs

Another technique to suppress subthreshold drain leakage current is to use a wide bandgap material as a backbarrier. A higher buffer potential prevents electrons from penetrating into the buffer and hence provides a better confinement. In this section the DC and transient pulsed simulation results of AlGaIn/GaN HEMTs with AlGaIn backbarrier will be discussed. Different thickness of the GaN channel layer d and Al mole fraction in AlGaIn backbarrier will be investigated.

4.4.1 DC characterisation

GaN Thickness

The thickness of the undoped GaN layer d was varied while the total thickness of the buffer was kept constant. Fig. 4.26b shows the energy diagram of

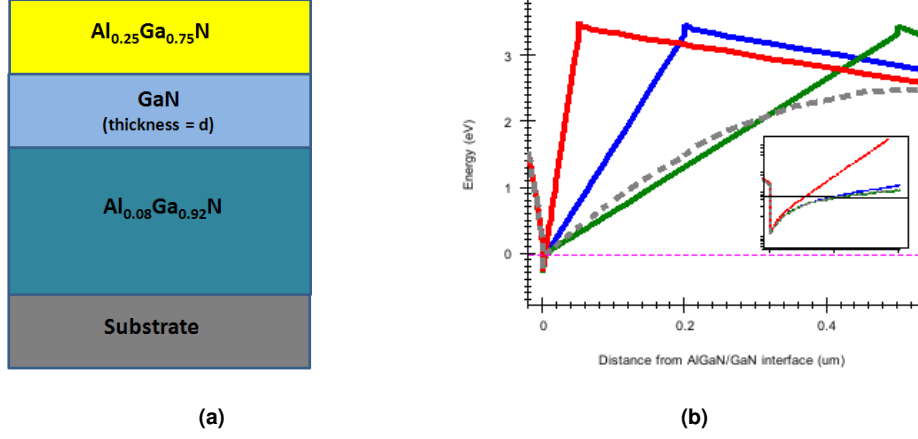


Figure 4.26: (a) Device structure with AlGaIn backbarrier (b) Energy diagram of conduction band for $d = 50$ nm (red), 200 nm (blue) and 500 nm (green). The inset shows a close up of energy band near the 2DEG.

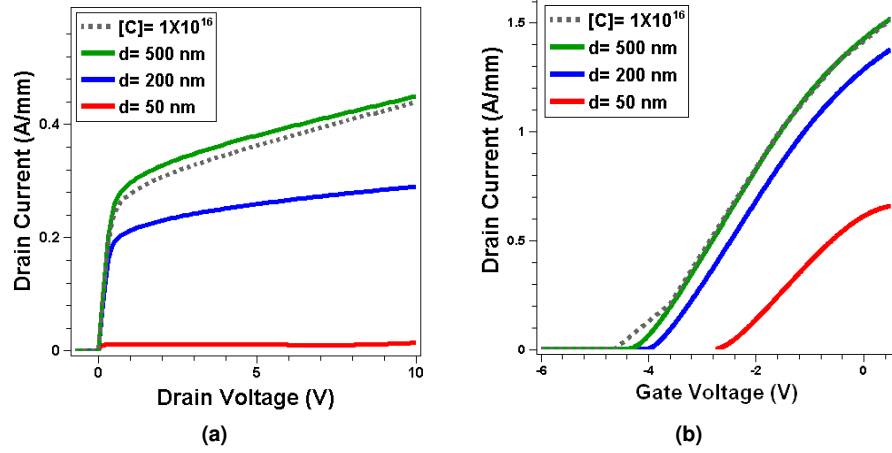


Figure 4.27: I-V curves for AlGaIn/GaN HEMTs with AlGaIn backbarrier (a) I_{ds} - V_{ds} at $V_{gs} = -3$ V (b) I_{ds} - V_{gs} at $V_{ds} = 10$ V

conduction band with AlGaIn backbarrier for $d = 50$ nm, 200 nm and 500 nm. The I-V curves are shown in Fig. 4.27.

As the thickness of GaN is decreased, the drain current decreases and the V_{th} increases. V_{th} is -2.47 V, -3.67 V and -3.98 V for $d = 50$ nm, 200 nm and 500 nm respectively. This is because for a thinner GaN layer, the wide band gap AlGaIn backbarrier is closer to the channel. This provides better electron confinement and results in higher threshold voltage. A more abrupt rise in potential however also decreases the size of the quantum well resulting in a lower electron density in the channel. As shown in the inset of Fig. 4.26b, the triangular region

enclosed by conduction band and Fermi level is smaller for $d = 50$ nm. Hence the electron density is smaller which results in a lower drain current.

Al mole fraction

Al mole fraction determines the bandgap of AlGa_xN. A higher Al content gives a wider bandgap. Fig. 4.28b shows the energy diagram of AlGa_xN/GaN/AlGa_xN HEMTs with 30%, 15% and 8% Al in the AlGa_xN-backbarrier. It can be seen that the energy bands for different Al content overlap in the GaN channel region but increase abruptly in the AlGa_xN backbarrier region.

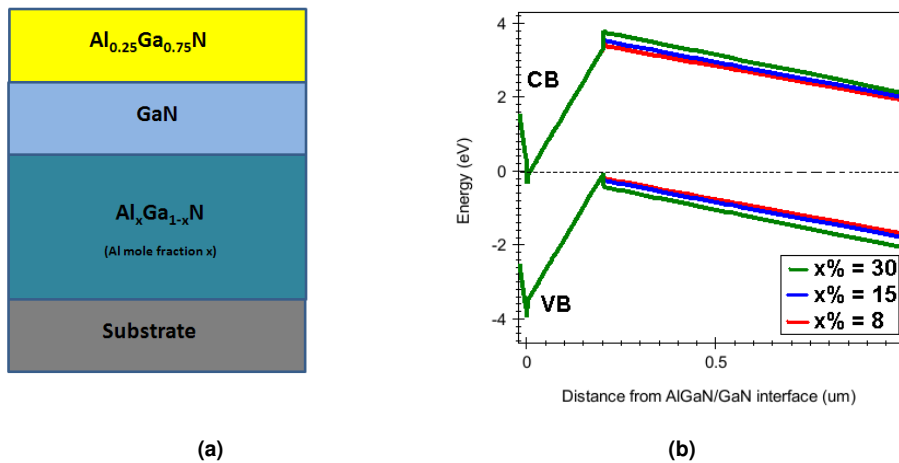


Figure 4.28: (a) Device structure with AlGa_xN backbarrier (b) Energy diagram for $x = 30\%$, 15% and 8% .

Fig. 4.29 shows the I-V characteristics for different Al content in the AlGa_xN backbarrier. It can be seen that there is not much difference in drain current. Since the energy band in the channel region overlap, this was an expected result. For a higher drain voltage in Fig. 4.29a it can be seen that the output resistance is higher with higher Al content. This is due to the higher potential barrier in the AlGa_xN region for higher Al content.

4.4.2 Transient pulsed simulation

Fig.4.30a shows the drain current for 200 nm and 500 nm thick GaN layer. In comparison to C doping, the current collapse is higher with AlGa_xN backbarrier. Fig. 4.30b shows the percentage current collapse. It can be seen that the current collapse is also higher for 200 nm than for 500 nm GaN layer.

These results were quite unexpected since there are no traps in the buffer. In this case, the decrease in current can be explained by considering the band diagram. In Fig. 4.31a it can be seen that although the potential is higher near the channel with AlGa_xN backbarrier, it gradually decreases in the buffer.

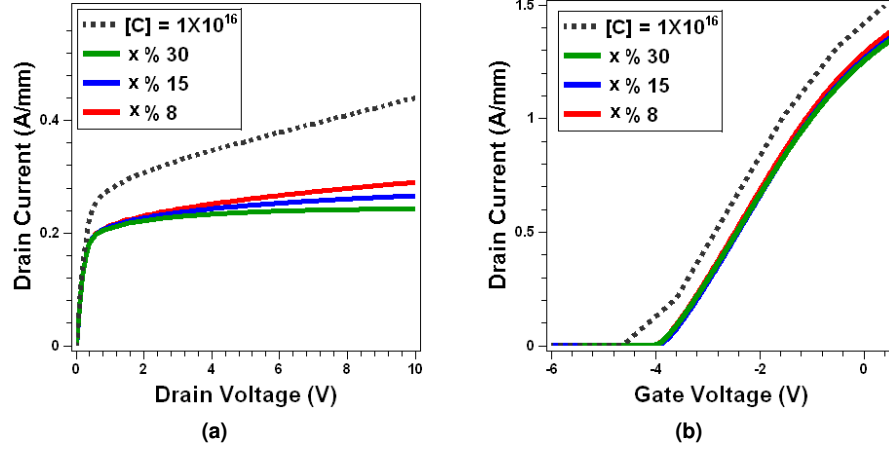


Figure 4.29: I-V curves for AlGaN/GaN/AlGaN HEMTs with different Al content in AlGaN backbarrier (a) I_{ds} - V_{ds} curves at $V_{gs} = -3$ V (b) I_{ds} - V_{gs} at $V_{ds} = 10$ V

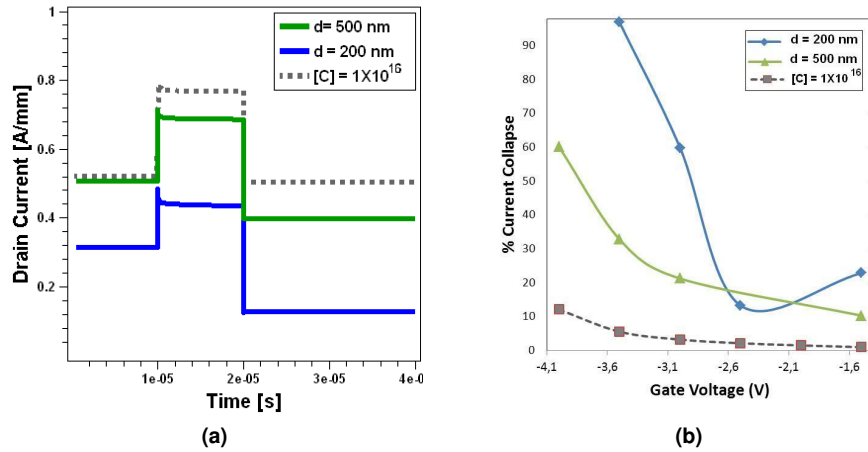


Figure 4.30: (a) Current collapse for different thickness of GaN layer at $V_{gs} = -3$ V. (b) Percentage current collapse as a function of V_{gs}

During the pulse, energetic electrons can overcome this potential barrier and then accumulate in the AlGaN/Substrate interface at the back as shown in Fig. 4.31b. Hence, it seems that with AlGaN backbarrier the device is very sensitive to the type of substrate used.

Another issue with AlGaN backbarrier is the formation of 2D hole gas. As it can be seen in Fig. 4.28b, the valence band is slightly higher than the fermi level at the GaN/AlGaN-backbarrier interface. The electron and hole density can be seen in Fig. 4.32. During the pulse, energetic electrons from the channel can recombine with the holes at the GaN/AlGaN-backbarrier interface resulting in loss of electrons. Doping the AlGaN region by donors has been used to increase

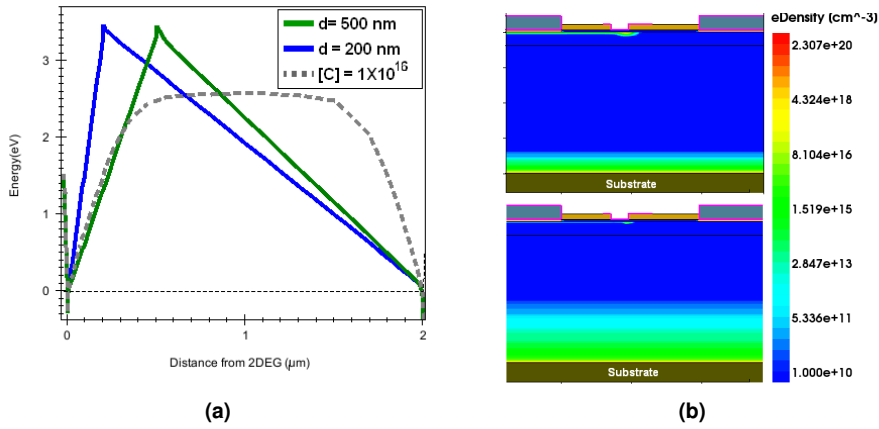


Figure 4.31: (a) Energy diagram for conduction band (b) Electron density before (top) and after (bottom) the pulse for $d = 500$ nm

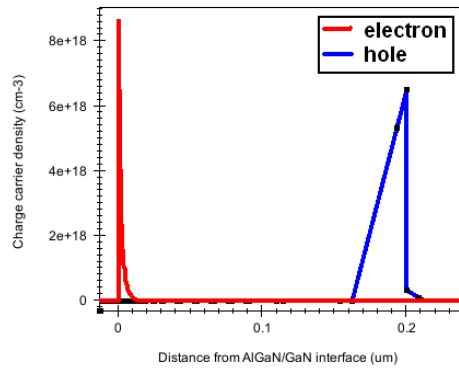


Figure 4.32: Electron and hole concentration as a function of distance from the AlGaIn/GaN interface

electron density and suppress the formation of 2DHG [34].

The thermal conductivity of AlGaIn is also lower than that of GaN. This raises additional concern of high self heating since these devices are operated at high temperatures [35].

Chapter 5

Conclusion

In this project, DC and transient pulsed characteristics were simulated for GaN based HEMTs. Different concentrations of C and Fe doping in the GaN buffer were investigated. It was found that doping can effectively suppress subthreshold drain leakage. A higher doping concentration resulted in a lower drain current, a higher threshold voltage and a higher output resistance. The current collapse was higher with Fe doping than C doping. For C doping, the current collapse decreased when the doping concentration was increased from $1 \times 10^{16} \text{ cm}^{-3}$ to $1 \times 10^{17} \text{ cm}^{-3}$ whereas it increased for Fe doping. This was because C traps have deeper energy levels and can increase the buffer potential to a higher level and provide better electron confinement.

AlGaIn/GaN HEMTs with an undoped GaN layer on top of $1 \times 10^{17} \text{ cm}^{-3}$ C doped GaN layer were investigated. A thicker undoped GaN layer resulted in a higher drain current, a lower threshold voltage and a lower output resistance. The current collapse was slightly worse for a thicker undoped layer. This is because with thicker undoped layer, fewer traps are filled before the pulse since they are further away from the channel.

AlGaIn/GaN HEMTs with AlGaIn backbarrier were also investigated. Devices with thicker GaN layer had higher drain current, lower threshold voltage and lower output resistance. Devices with higher Al content in the AlGaIn-backbarrier had a higher output resistance but the drain current and the threshold voltage were similar for all cases. The current collapse with AlGaIn backbarrier was higher than with C doped GaN buffer. The reason for this was the lower potential barrier at the AlGaIn/Substrate interface which resulted in accumulation of electrons at the back during pulse.

Among the three different device structures simulated, devices with an undoped GaN channel on $1 \times 10^{17} \text{ cm}^{-3}$ C doped GaN buffer showed the best performance. The current collapse in these devices was very small but the drain current was a lot higher. In the future it would be interesting to see more simulation results with thermal effects. Also, in literature it is said that hot electron injection plays an important role in current collapse [34]. Therefore, Hydrodynamic simulation which take into account hot electron effects could give some new insight.

Acknowledgements

I would like to thank my supervisors Dr. Hans Hjelmgren and Dr. Mattias Thorsell and my examiner Dr. Niklas Rorsman. This work would not have been possible without their continuous guidance and support. I would specially like to thank Dr. Hans Hjelmgren for introducing me to TCAD simulations and for showing incredible patience.

I would also like to thank Qiaoran Yang for valuable discussions, Mehbuba Tanzid Mihika for proof reading the thesis, Jan Andersson and Henrik Fjellstedt for the IT support and everyone in Microwave Electronics Laboratory for creating a friendly atmosphere.

References

- [1] M. A. Khan, A. Bhattarai, J. N. Kuznia, and D. T. Olson, "High electron mobility transistor based on a GaN/AlGa_N heterojunction," *Appl. Phys. Lett.*, vol. 63, no. 1214, 1993.
- [2] R. S. Pengelly, S. M. Wood, J. W. Milligan, S. T. Sheppard, and W. L. Pribble, "A review of GaN on SiC high electron-mobility power transistors and MMICs," *IEEE Transactions on Microwave Theory and Techniques*, vol. 60, no. 6, 2012.
- [3] U. K. Mishra, P. Parikh, and Y.-F. Wu, "AlGa_N/Ga_N HEMTs: An overview of device operation and applications," *Proceedings of the IEEE*, vol. 90, no. 6, 2002.
- [4] S. C. Binari, P. B. Klein, and T. E. Kazior, "Trapping effects in GaN and SiC microwave FETs," *Proceedings of the IEEE*, vol. 90, no. 6, 2002.
- [5] S. Suihkonen, "Phd thesis ingan quantum wells for led applications," *Helsinki University of Technology*, 2008.
- [6] A. Zoroddu, F. Bernardini, and P. Ruggerone, "First-principles prediction of structure, energetics, formation enthalpy, elastic constants, polarization, and piezoelectric constants of AlN, GaN, and InN: Comparison of local and gradient-corrected density-functional theory," *Physical Review B*, vol. 64, no. 045208, 2001.
- [7] M. Koèan, "AlGa_N/Ga_N MBE 2DEG heterostructures: Interplay between surface, interface and device properties," *Rheinisch-Westfälische Technische Hochschule, Aachen, PhD Thesis*, 2003.
- [8] F. Bernardini, V. Fiorentini, and D. Vanderbilt, "Spontaneous polarization and piezoelectric constants of III-V nitrides," *Physical Review B*, vol. 56, no. 16, 1997.
- [9] O. Ambacher, J. Smart, J. R. Shealy, N. G. Weimann, K. Chu, M. Murphy, W. J. Schaff, L. F. Eastman, R. Dimitrov, L. Wittmer, M. S. W. Rieger, and J. Hilsenbeck, "Two-dimensional electron gases induced by spontaneous and piezoelectric polarization charges in N- and Ga-face AlGa_N/Ga_N heterostructures," *J. Appl. Phys.*, vol. 85, no. 3222, 1999.
- [10] I. P. Smorchkova, C. R. Elsass, J. P. Ibbetson, R. Vetury, B. Heying, P. Fini, E. Haus, S. P. DenBaars, J. S. Speck, and U. K. Mishra, "Polarization-induced charge and electron mobility in AlGa_N/Ga_N heterostructures

- grown by plasma-assisted molecular-beam epitaxy," *J. Appl. Phys.*, vol. 86, no. 4520, 1999.
- [11] I. P. Smorchkova, L. Chen, T. Mates, L. Shen, S. Heikman, B. Moran, S. Keller, S. P. DenBaars, J. S. Speck, and U. K. Mishra, "AlN/GaN and AlGa_N/AlN/GaN two-dimensional electron gas structures grown by plasma-assisted molecular-beam epitaxy," *J. Appl. Phys.*, vol. 90, no. 5196, 2001.
- [12] E. T. Yu, G. J. Sullivan, P. M. Asbeck, C. D. Wang, D. Qiao, and S. S. Lau, "Measurement of piezoelectrically induced charge in GaN/AlGa_N heterostructure field-effect transistors," *Appl. Phys. Lett.*, vol. 71, no. 2794, 1997.
- [13] E. Zurich. (2013, 06) High electron mobility transistors (hemt). [Online]. Available: <http://www.mwe.ee.ethz.ch/en/about-mwe-group/research/vision-and-aim/high-electron-mobility-transistors-hemt.html>
- [14] D. Balaz, "Current collapse and device degradation in AlGa_N/GaN heterostructure field effect transistors. PhD thesis," *University of Glasgow*, 2011.
- [15] S. Dunham. (2013, May) Notes on semiconductor devices in nonequilibrium. [Online]. Available: <http://dunham.ee.washington.edu/ee482/Notes/Nonequil.pdf>
- [16] S. Inc. (2013, 06) Tcad. [Online]. Available: <http://www.synopsys.com/Tools/TCAD/Pages/default.aspx>
- [17] D. Pennicard. (2013, 06) Introduction to sentaurus TCAD. [Online]. Available: <http://www.docstoc.com/docs/105963452/Introduction-to-Sentaurus-TCAD>
- [18] B. Danilchenkoa, I. Obukhova, T. Paszkiewicz, S. Wolskib, and A. Jezowski, "On the upper limit of thermal conductivity GaN crystals," *Solid State Communications*, vol. 144, no. 3/4, pp. 114–117, 2007.
- [19] S. G. Müller, J. J. Sumakeris, M. F. Brady, R. C. Glass, H. M. Hobgood, J. R. Jenny, R. Leonard, D. P. Malta, M. J. Paisley, A. R. Powell, V. F. Tsvetkov, S. T. Allen, M. K. Das, J. W. Palmour, and C. H. C. Jr., "Defects in SiC substrates and epitaxial layers affecting semiconductor device performance," *Eur. Phys. J. Appl. Phys.*, vol. 1-3, no. 29-35, 2004.
- [20] S. G. Müller, R. C. Glass, H. M. Hobgood, V. F. Tsvetkov, M. Brady, D. Henshall, D. Malta, R. Singh, J. Palmour, and C. H. C. Jr., "Progress in the industrial production of SiC substrates for semiconductor devices," *Mater. Sci. Eng. B*, vol. 1-3, no. 327-331, 2001.
- [21] A. S. Barker and M. Ilegems, "Infrared lattice vibrations and free-electron dispersion in GaN," *Phys. Rev. B*, vol. 7, no. 2, pp. 743–750, 1973.
- [22] W. J. Moore, J. A. F. Jr., R. T. Holm, O. Kovalenkov, and V. Dmitriev, "Infrared dielectric function of wurtzite aluminum nitride," *Appl. Phys. Lett.*, vol. 86, no. 14, 2005.

- [23] L. Gordon, M.-S. Miao, S. Chowdhury, M. Higashiwaki, U. K. Mishra, and C. G. V. de Walle, "Distributed surface donor states and the two-dimensional electron gas at AlGa_N/Ga_N heterojunctions," *J. Phys. D: Appl. Phys.*, vol. 43, no. 50, 2010.
- [24] A. W. Smitha and K. F. Brennanb, "Hydrodynamic simulation of semiconductor devices," *Progress in Quantum Electronics*, vol. 21, no. 4, 1998.
- [25] W. Fichtner, D. J. Rose, and R. E. Bank, "Semiconductor device simulation," *IEEE Transaction on electron devices*, vol. 30, no. 9, 1983.
- [26] R. Trew, "SiC and GaN transistors - is there one winner for microwave power applications?" *Proceedings of the IEEE*, vol. 90, no. 6, pp. 1032–1047, 2002.
- [27] H. Hjelmgren, M. Thorsell, K. Andersson, and N. Rorsman, "Extraction of an electrothermal mobility model for AlGa_N/Ga_N heterostructures," *IEEE Transactions on Electron Devices*, vol. 59, no. 12, pp. 3344–3349, 2012.
- [28] O. Lopatiuk, L. Chernyak, Y. Feldman, and G. K, "Studies of electron trapping in Ga_N doped with carbon," *Thin solid films*, vol. 515, no. 10, pp. 4365–4368, 2007.
- [29] J. Baur, K. Maier, M. Kunzer, U. Kaufmann, and J. Schneider, "Determination of the Ga_N/Al_N band offset via the (-/0) acceptor level of iron," *Applied Physics Letters*, vol. 65, no. 2211, 1994.
- [30] J. L. Lyons, A. Janotti, and C. G. V. de Walle, "Carbon impurities and the yellow luminescence in Ga_N," *Applied Physics Letters*, vol. 97, no. 152108, 2010.
- [31] A. Y. Polyakov, N. B. Smirnov, A. V. Govorkov, A. A. Shlensky, K. McGuire, E. Harley, L. E. McNeil, R. Khanna, S. J. Pearton, and J. M. Zavada, "Properties and annealing stability of Fe doped semi-insulating Ga_N structures," *Physica Status Solidi (C)*, vol. 2, no. 7, pp. 2476–2479, 2005.
- [32] J. Bourgoin, "Point defects in semiconductors," 1983.
- [33] "Sentaurus device user guide," vol. Version G-2012.06, 2012.
- [34] W. D. Hu, X. S. Chen, F. Yin, J. B. Zhang, and W. Lu, "Two-dimensional transient simulations of drain lag and current collapse in Ga_N-based high-electron-mobility transistors," *J. Appl. Phys.*, vol. 105, no. 084502, 2009.
- [35] W. Liu and A. A. Balandin, "Thermal conduction in AlGa_N alloys and thin films," *J. Appl. Phys.*, vol. 97, no. 7, 2005.